1
2
3
4
5
6
7
8
9
10
11
12
13
14
15
16
17
18
19
20
21
22
23
24
25
26
27
28
29
30
31
32
33
34
35
36
37
38
39
40
41
42
43
44
45
46
47
48
49
50
51
52
53
54
55
56
57
58
59
60

Water Retention Characteristics of Swelling Clays in Different Compaction States

Kannan K. R Iyer[a,b*], Jeevan Joseph[c], B. C. F. L Lopes[d,e], D. N. Singh[f]

and Alessandro Tarantino[g]

For Peer Review Only

----

[a]Formerly Research Scholar, Department of Civil Engineering, Indian Institute of Technology Bombay, Powai, Mumbai-400076, India

[b]Assistant Professor, Department of Civil Engineering, Institute of Infrastructure Technology Research and Management, Near Khokhra circle, Ahmedabad-380026, India, kannaniyer@iitram.ac.in

*Corresponding author. Tel.: +91-9833427915

[c]Research Scholar, Department of Civil Engineering, Indian Institute of Technology Bombay, Powai, Mumbai-400076, India, jeev.jsph@gmail.com

[d]Formerly Research Scholar, Department of Civil and Environmental Engineering, University of Brasilia, Brasilia, Brazil

[e]Associate Research, Department of Civil and Environmental Engineering, University of Strathclyde, James Weir Level 5, 75 Montrose Street, Glasgow G1 1XJ, bfarialima@gmail.com

[f]Institute Chair Professor, Department of Civil Engineering, Indian Institute of Technology Bombay, Powai, Mumbai-400076, India, dns@civil.iitb.ac.in

[g]Professor, Department of Civil and Environmental Engineering, University of Strathclyde, James Weir Level 5, 75 Montrose Street, Glasgow G1 1XJ, alessandro.tarantino@strath.ac.uk

ABSTRACT

The soil water retention (SWR) characteristics of the clays play an important role in controlling their engineering behaviour, particularly, in the unsaturated state. Although, researchers have attempted to understand the water retention characteristics of the clays in their reconstituted or remoulded state, such studies are rare for the clays in their intact state. In this context, it becomes important to understand the influence of initial state of compaction, which would create different pore- and fabric- structure (viz., microstructure), on the water retention characteristics of the clays. With this in view, SWR behaviour was determined experimentally for the swelling clays (dried from different compaction states, viz., intact, reconstituted and remoulded) by employing Dewpoint Potentiameter (WP4C®). The changes in the pore-size distribution of the clays at different stages of drying cycle were also studied by employing the Mercury Intrusion Porosimetry. The study reveals that the SWR curves for the intact and reconstituted specimens of the clays converge beyond a certain stage of drying. Also, a critical analysis of changes in the pore structure of the swelling clay specimens, during drying, indicates that the progressively deforming pore structure play an important role in controlling its water retention characteristics to a great extent.

KEYWORDS: swelling clays, state of compaction, soil-water retention curve, Dew point Potentiameter, microstructural studies.

Introduction

The uniqueness of the soil water retention curve, SWRC, has been studied by earlier researchers and it has been reported that it gets influenced by various factors such as the soil type (Fredlund et al. 2002, Pham *et al*. 2005, Frydman and Baker 2009, Noh *et al.* 2011), water

content and compaction efforts (Tinjum et al. 1997, Vanapalli et al. 1998, 1999; Charles and Pang 2000a, 2000b; Miller et al. 2002, Sreedeep and Singh 2005, Thakur *et al.* 2005, 2006), initial void ratio (Kawai et al. 2000), stress history (Delage and Lefebvre 1984, Vanapalli et al. 1998, 1999; Charles and Pang 2000a, 2000b; Marinho 2005), and the path viz., drying- or wetting- path, adopted to achieve it (Likos and Lu 2002, Yang et al. 2004, Pham *et al.* 2005, Agus and Schanz 2006, Konyai *et al.* 2006, Mohammed and Sharma 2007, Fredlund *et al.* 2011, Jayanth *et al.* 2012). Incidentally, earlier studies have also noted the effect of initial state of soil (intact, slurried or compacted) on its SWRC (Fredlund et al., 2002; Pham et al., 2008). These studies indicate that the water retention characteristics of compacted specimens are different as compared to intact and slurried specimens. Further, it was also suggested that the SWRC for intact and slurried specimens are comparable beyond suction of about 1 MPa (Pham et al., 2008). The differences in the water retention behaviour for intact, reconstituted (read slurried) and compacted (read remoulded) specimens of the same soil, can be attributed to difference in the soil microstructure and initial water content.

In this context, some studies were also aimed at understanding the relationship between the microstructure of the soil and its water retention behaviour (Romero et al, 1999). It was observed, from this study on compacted boom clay, that for water content above 15%, the main drying and wetting path SWRCs depends on the void ratio and with increase in dry density of soil, the air-entry value also increases. However, it was reported that the SWRCs do not depend on the dry density of the soil, for water content ranging from 5-15 %, and further it was noted that for dry soils (viz., water content less than 5%), the drying- and wetting- path SWRCs converge. It was also concluded that the water retention behaviour of soil is directly controlled

by the microstructure, mainly by the water present in the inter-aggregate pores during the initial compaction.

Some studies have attempted to understand the evolution in soil microstructure during compaction process, and have suggested that the compaction process results in reduction of inter-aggregate pores (macro pores), whereas there is insignificant effect on the intra-aggregate pores (Shidharan et al., 1971; Delage, 2009). Diamond (1971) based on studies on Kaolin and Illite clay concluded that samples compacted at dry of optimum exhibited aggregation with micro-pores and inter-aggregate macro-pores. However, for samples compacted at or on wetside of optimum moisture content, the microstructural features were nearly massive structure consisting of domains (aggregation of clay particles) mostly in mutual contact with each other. A study by Djeran-Maigre et al. (1998) reveals that remoulded clay samples have randomly oriented particles. However, with increasing compaction pressure, the fabric structure becomes more oriented and interparticle pores disappear mainly due to face to face contact of the clay particles.

Further, the effect of water content on microstructure of compacted soils has been studied by some researchers (Ahmed et al., 1974; Prapaharan et al., 1991; Delage et al., 1996; Tarantino and De Col, 2008), where clays are noticed to exhibit 'mono-modal pore size distribution' when compacted wet of optimum or at optimum water content. These clays were noticed to exhibit 'bi-modal pore size distribution' when compacted dry of optimum water content. Tanaka et al. (2003) have observed that natural silty and clayey soils exhibit 'mono-modal pore size distribution'. However, Gracia-Bengochea et al. (1979) have demonstrated that for the soils with higher silt content, even samples compacted on wet side of optimum may exhibit 'bi-modal pore size distribution', where the larger cluster of the pores represent inter-aggregate pores and smaller cluster of pores represent the intra-aggregate pores. The 'Bi-modal pore size distribution'

has also been reported in saturated clays corresponding to their over-consolidated state (Ninjgarav et al., 2007).

Researchers have also focused on the microstructural changes during drying for the compacted soils. Cuisinier and Laloui (2004) have revealed that soils compacted at different water contents, when subjected to drying, exhibit reduction in their macro- and micro- pore volumes; however the dominant macro- and micro- pore sizes remained mostly unchanged. Some studies on the soils compacted on wet side of the optimum, reveal 'mono-modal pore size distribution', initially, which subsequently gets evolved into 'bi-modal pore size distribution', on drying (Gens et al., 1995; Simms and Yanful, 2001). However, opposite inferences have been reported by Cuisinier and Laloui (2004); wherein the shrinkage of larger pores and transformation of initial 'bi-modal pore size distribution' to 'mono-modal pore size distribution' has been observed during drying.

Some researchers have studied the evolution of aggregate size with change in water content during wetting cycles. Romero et al. (2011) studied the microstructural evolution for clayey soil and have observed that the clay compacted on dry side of optimum initially exhibits bimodal pore size distribution, however on saturation during wetting cycle; the microstructure evolves to mono-modal pore size distribution. Interestingly, when the soil is subjected to subsequent drying cycle, the bi-model pore size characteristics are recovered. Moreover, the researchers' observed that the inter-aggregate pore size and volume reduces during saturation of the compacted clay, however the aggregation created during soil compaction remains permanent feature of the soil microstructure. Seiphoori et al. (2014) have reported an irreversible alteration in the water retention behaviour of bentonite used in engineered barrier systems, as the water content approaches saturation during the first wetting cycle. The role of microstructure evolution

has been highlighted and it has been noted that the volume of macro-pores reduces and no remarkable change is observed in the volume of micro-pores. This microstructural evolution has been attributed by the researchers' to expansion of the aggregates causing reduction in the macro-pore size and volume; and resulting in a more homogenous and compact structure.

Some studies have attempted to understand the variation in soil microstructure for different initial states of compaction (viz., compacted, reconstituted, intact). Monroy et al. (2010) have reported based on studies on compacted and reconstituted clay, that on application of loading or hydration of soil samples (wetting cycles), both compacted and reconstituted clay samples exhibit mono-modal pore size distribution. However, reconstituted samples exhibited lower entrance dominant pore diameter as compared to compacted samples. Another study by Hattab et al. (2013), based on the microstructural evolution of deep marine clay sediments along different stress paths, concluded that for the remoulded (read compacted) marine clays the inter-aggregate pore volume decreases mainly due to the aggregate sliding mechanism, while intra-aggregate pore volume remains unaffected. However, for the intact (read undisturbed) samples of clays from the marine deposits, the aggregate sliding mechanism is retarded due to bonding (read self-weight consolidation, refer Gumaste et al. 2014a, b) between the aggregates. Burton et al. (2015) studied the microstructural changes of high plasticity clay subjected to wetting and drying cycles from different initial compaction states, and observed that there is good agreement in the micro-pore range for the compacted, reconstituted and undisturbed samples of the clay. Further, the researchers' observed that under oedometric conditions, the bi-modal pore size distribution of compacted clay sample gets altered during saturation and resembles the microstructure of reconstituted sample. Moreover, it has been reported that the initial bio-modal pore size distribution is not recovered when the compacted clay sample is dried from saturated state.

In spite of numerous studies, Tarantino (2011) observed that many concepts developed for unsaturated soils are based on the studies related to the compacted soils with 'bimodal pore size distribution'. It was also noted that the compacted samples exhibit larger inter-aggregate pores as compared to intra-aggregate pores, due to presence of large aggregates. In contrast, in reconstituted samples, the inter-aggregate and intra-aggregate pores may be of comparable sizes, and the pore size distribution may appear as 'mono-modal'. It was further suggested that as the compaction water content decreases, the size of aggregation reduces; however the size of inter-aggregate pores increase. Thus compaction water content significantly influences the fabric structure of the compacted soils.

It has been realized that the existing studies deal with, mainly, non-swelling type soils in their compacted (read remoulded) state and not much attention has been paid by the researchers to understand the micro-structure of the soils in their reconstituted (read slurried) and the intact (read undisturbed) states. Also, the mechanisms responsible for the difference in the soil water retention curves, SWRCs, of the soil during drying from different initial states of compaction, and the difference in the microstructural evolution, needs to be established. With this in view, drying path SWRCs of the clays that exhibit swelling were developed by varying the initial state of compaction (viz., intact, reconstituted and compacted). This was followed by the investigations related to the microstructural changes occurring at different stages of drying-path, as described in this paper.

Experimental Investigations

Properties of the Swelling Clay

Naturally occurring swelling clay, designated as SC1, collected from the western region of India was considered in the present study. The clay was characterized to establish its physical and mineralogical properties. The grain size distribution (ASTM D 422-94), consistency limits (ASTM D 4318-05 and ASTM D 427-98), specific gravity G_s (ASTM D 5550-06) and free swell Index, *FSI*, (IS: 2720, Part XL) of the clay were determined and the results are presented in Table 1. The clay can be characterized as CH as per the Unified Soil Classification System (ASTM D 2487-06e1). The specific surface area, *SSA*, of the clay was determined by conducting Ethylene Glycol Monoethyl Ether Absorption (EGME) test, based on the recommendations available in the literature (Arnepalli *et al.* 2008). The mineralogical composition of the clay SC1 was determined with the help of X-ray Diffraction (XRD) Spectrometer (Manufacturer: PANalytical X'Pert PRO), which employs a graphite monochromator and Cu-Kα radiation. The clayey sample was scanned from 2θ ranging from 5° to 80°. The major minerals present in the clayey sample are also listed in Table 1.

Establishment of the SWRC

In order to establish the drying-path SWRC of the clay SC1, in its undisturbed state, referred as intact state and designated as **I**, specimens were extracted from the Shelby tubes by using cylindrical stainless steel cutting-edge rings of inner diameter 35.5 mm and height 7 mm. These specimens were placed in the PVC cups (with a lid) provided by the manufacturer of dewpoint potentiameter (WP4C®), which was used for measuring the total suction and subsequently developing the drying-path of the SWRC (Iyer et al. 2013), designated as SWRC-**I**.

To achieve this, weight of the specimen was recorded at each stage of drying to obtain the gravimetric water content of the specimen corresponding to certain suction. After completion of the tests on the undisturbed specimens, they were air dried, pulverized carefully with the help of mortar and pestle to break the clay aggregation and were utilized for establishing the SWRC of the reconstituted specimens (designated as **R**) as explained in the following.

The reconstituted specimens were prepared by maintaining the initial moisture content close to the liquid limit, w_l, of the clayey soil and correspond to the slurried state of the clay. In this context, Jayanth *et al.* (2012) have demonstrated that such specimens are quite handy for suction measurements and establishment of the SWRC (designated as SWRC-**R**). Subsequently, the slurry was poured into the PVC cups and a specimen of about 5 mm thickness (WP4C Operator Manual, 2010) was obtained. The process of establishing drying path SWRC for the reconstituted specimens is similar to that of undisturbed specimens as explained earlier.

For drying tests on the compacted specimens (designated a **C**) of the clay , the air dried and pulverized samples were compacted at 21% (dry density, γ_d ~ 1.65 g/cc) and 25% water content (γ_d ~ 1.56 g/cc), by employing a miniature compactor (Kolay and Singh, 2000), which resembles static compaction method with kneading action. These samples are designated as C21and C25, respectively. Incidentally, these moisture contents are close to the plastic limit, w_p, of the clayey soil. Subsequently, specimens were extracted from the compaction mold (Thakur et al. 2006), and drying-path SWRC (designated as SWRC-**C**) was established.

Each of these SWRCs were replicated twice (designated as trials T1 and T2) so as to eliminate the effect of material heterogeneity and human errors.

Results

In order to demonstrate the influence of the initial state of the clayey specimen on its SWRC, the SWRC-**I**, SWRC-**R** and SWRC-**C** were superimposed as depicted in Fig. 1. In this context, the specimens (refer Fig. 2) are designated as I1 to I4, R1 to R4, C21 and C25, corresponding to the intact, reconstituted and compacted states, respectively. The suffixes P1 and P2, associated with C21 and C25, correspond to the specimens just after compaction (i.e., before air-drying) and at maximum possible air-drying stage, respectively. The P2 stage was arrived at by weighing the specimens and making sure that three consecutive values of the weight (measured at 24 hour time interval) remain unchanged. The suction values and corresponding water content of the intact, reconstituted and compacted specimens are presented in Table 5. From the Fig. 1 it can be noticed that the SWRCs for the intact and reconstituted specimens, defined as **I** and **R**, respectively, converge at a suction, ψ_c, close to 2 MPa. Such a response of the clay might be hypothesized to either (a) loss of 'clay-microstructure effect', beyond ψ_c, which otherwise would have governed the capillary component of the suction. In such a case, the capillary component of suction, which depends on the clay microstructure, no more influences the SWRC and the adsorptive surface forces (viz., van der Waals surface forces) control the water retention behaviour of soils (Tuller and Or, 2005). This phenomenon may be expressed as loss of 'clay-microstructure effect'. As such, the water retention characteristics of the clay becomes independent of the initial state of the clay (viz., undisturbed natural formation or reconstituted state) and/or (b) deformability (i.e., the shrinkage) of the pores during drying process which might result into similar pore-size distribution for the intact and reconstituted states, close to ψ_c. With context to hypothesis (a), it is worth mentioning here that earlier studies have noted that the capillary component of suction becomes insignificant beyond/close to 10

MPa (Tuller and Or, 2005). However, as this observation has been reported based on the studies related to non-swelling soils, its applicability for swelling clay(s) needs to be ascertained. It should also be noted that the initial portion of SWRC for intact and reconstituted specimens (refer Fig. 1) is comparable to the initial compression line (viz., relationship between void ratio and soil effective stress) usually obtained from consolidation test of saturated soil mass under external loading (Ridley and Romero, 1998). In both these processes, the reduction in volume of soil is a result of expulsion of water without replacement by air (consolidation) as a result of an increase in the effective stress. The change in slope of SWRC for both intact and reconstituted specimens at around 2 MPa (incidentally at this suction, the SWRC of these two specimens converge), indicates the point of desaturation. This suggests that specimens I1, I2, R1 and R2 are saturated, and the beginning of desaturation for intact specimens happens at drying stage between I2 and I3, whereas for reconstituted specimens desaturation begins at drying stage between R2 and R3. Further, as depicted in Fig. 1, the SWRC-**C** falls under the SWRC-**I** and SWRC-**R**, which might be attributed to the fact that the compaction of the clays controls the microstructure of the specimen (Li and Zhang, 2009).

In order to validate the above mentioned hypotheses, the microstructure of the specimens corresponding to different stages of drying, after measuring their suction, was established by resorting to the Mercury Intrusion Porosimetry, MIP tests.

The variation of cumulative void ratio, e_{MIP} (computed from cumulative volume of mercury intruded in the specimen, V_{Hgc}, by employing Eqn. 1), and incremental void ratio, $-\Delta e_{MIP}/\Delta(\log d)$ with respect to the pore-diameter, d, was plotted as depicted in Figs. 3 to 8. The cumulative void ratio, e_{MIP}, is given by

$$e_{MIP} = \frac{V_{Hgc}}{\left(\frac{M_s}{\varrho_s}\right)} \tag{1}$$

where, e_{MIP} is the cumulative void ratio of the specimen, V_{Hgc} is the cumulative volume of mercury intruded in the specimen (cm^3), M_s is the dry mass of clay specimen (g), and ρ_s is the density of the solids (g/cm^3).

It should be noted that cumulative void ratio curve has been fitted by employing the modified van Genuchten equation (Dieudonne et al., 2014; Lopes et al., 2014), represented by Eqn. 2.

$$ e = p_m \left(\frac{1}{1+\left(\alpha_m d\right)^{n_m}} \right)^{1-\frac{1}{n_m}} + p_M \left(\frac{1}{1+\left(\alpha_M d\right)^{n_M}} \right)^{1-\frac{1}{n_M}} \tag{2} $$

where e is the cumulative void ratio (estimated) from modified van Genuchten model; d is the pore diameter; p, α and n are the model fitting parameters; m and M refer to intra-aggregate and inter-aggregate porosity, respectively for dual porosity structure. In case of mono-modal pore size distribution, only one set of parameters would be required to define the pore size distribution. The parameter 'p' is related to the total cumulative volume and the frequency of the dominant pore diameter; the parameter 'n' is related to the slope of the cumulative intrusion curve at the inflection point, and hence also controls the frequency of the dominant pore diameter; whereas, parameter 'α' is approximately related to inverse of the dominant pore diameter and controls inflection point of the intrusion curve (Lopes et al., 2014).

The derivative of Eqn. 2 yields the incremental void ratio, $-\Delta e /\Delta(\log d)$, as recommended by Lopes et al. 2014, and is expressed by Eqn. 3.

$$ \frac{\Delta e}{\Delta(\log d)} = \frac{p_m.n_m.\left(\alpha_m d\right)^{n_m}.\left(1-\frac{1}{n_m}\right).\left(\frac{1}{1+\left(\alpha_m d\right)^{n_m}}\right)^{1-\frac{1}{n_m}}}{\left(1+\left(\alpha_m d\right)^{n_m}\right)} + \frac{p_M.n_M.\left(\alpha_M d\right)^{n_M}.\left(1-\frac{1}{n_M}\right).\left(\frac{1}{1+\left(\alpha_M d\right)^{n_M}}\right)^{1-\frac{1}{n_M}}}{\left(1+\left(\alpha_M d\right)^{n_M}\right)} \tag{3} $$

Studies by Lopes et al. (2014) suggested that Eqn. 2 can be used for fitting the cumulative pore size distribution of soils. This has been confirmed in the present study, wherein Eqn. 2 has been found to provide good fitting of the cumulative pore size distribution for swelling clay specimens (refer Fig. 9 which depicts fitting of cumulative void ratio for specimens I3 and R3). The parameters p, α and n are varied during an iterative process to obtain the best fit curve for the cumulative pore size distribution data (Cumulative void ratio vs pore diameter). The plot of $-\Delta e/\Delta \log(d)$ obtained from Eqn. 3 and the corresponding pore diameter (d), gives the incremental pore size distribution curve, as shown in Figs. 4, 6 and 8.

It can be noted from the Figs. 4 and 8 that the intact and compacted specimens depict bimodal pore size distribution (viz., group of inter-aggregate pores and intra-aggregate pores) with two distinct groups of pore sizes ; whereas reconstituted specimens depict mono-modal pore size distribution (refer Fig. 6). Table 2 presents the percentage inter-aggregate and intra-aggregate pores and the dominant pore diameter (Souli et al., 2008) for intact and compacted specimens, obtained by employing the modified van Genuchten bimodal equation, refer Eqn. 3 (Dieudonne et al., 2014; Lopes et al., 2014). Except when a sharp peak is observed in incremental pore size distribution curve, viz., specimen R1 (refer Fig. 6), the dominant pore diameter is represented as a range (refer Table 2) with lower and upper limit values indicating the pore diameter on either side of peak value, and the average value of dominant pore diameter is also presented in Table 2. The first part of Eqn. 3 yields the intra-aggregate pore fraction, whereas the second part yields the inter-aggregate pore fraction.

It can be seen from Table 2 that for the intact clay specimens, the average dominant pore size of the intra-aggregate pores, d_{d1}, as well as the average inter-aggregate pore size, d_{d2}, reduces during the drying process. The proportion of intra-aggregate pores increases with

corresponding reduction in the proportion of inter-aggregate pores. Interestingly, the pore size distribution, which was bi-modal initially, remains bi-modal during the drying process. Further, the intra-aggregate voids ratio reduces during the drying process (Table 2), which indicates the shrinkage of aggregates and narrowing of the intra-aggregate pores. Incidently, the inter-aggregate voids ratio also reduces during the drying cycle, indicating shrinkage of these pores. The shrinkage of inter-aggregate pores suggests their initial saturated state, as explained later in Fig. 13. Further, from Table 2 it can also be observed that for compacted specimens, the average intra-aggregate pore size reduces during drying. Although the volume of intra- and inter-aggregate pores reduces during drying, the proportion of intra- aggregate pores reduces and the proportion of the inter-aggregate pores increased. The reduction in intra-aggregate voids ratio for the compacted specimens indicates aggregate shrinkage mechanism during drying similar to that for intact specimens.

For reconstituted specimens (refer Table 3), average dominant pore size reduces from 4.10 μm for specimen R1 to 0.092 μm for specimen R2. The air dried specimen, R4 exhibits average dominant pore size of 0.007 μm. Such significant reduction in the pore sizes indicates shrinkage and closure of pores from initial slurried condition. As aggregation effect is expected to be absent in initial slurried specimens, the pore size distribution of initial slurried specimen cannot be classified as intra-aggregate or inter-aggregate pores. During the drying process, shrinkage of specimen and formation of the small aggregations may result in both intra- and inter- aggregate pores. However, researchers have noted that the mono-modal pore size distribution observed in reconstituted specimens with comparable intra- and inter- aggregate pore sizes, makes it extremely difficult to distinguish between the two families of pores (Tarantino, 2011). It should be noted that some larger size pores observed for specimens R2 and R3 in Fig. 6

can be concluded as artifacts; since this range of pore sizes are missing in initial slurried state represented by R1. These artifacts might be a result of micro-cracking during the freeze drying process or during the drying process of the specimen itself, and hence have been ignored.

Further, to understand the process of de-saturation and shrinkage of the pores during drying, the water ratio, e_w (viz., ratio of volume of water in the pores to volume of solids) at each stage of drying has been computed by employing the volume-mass relationship ($e_w=w.G$, where G = specific gravity of soil specimen) and compared with the total void ratio, e (Tarantino, 2011; Romero et al., 2011). A fully saturated clay would indicate that $e_w=e$, which suggests that all the pores are saturated. Table 4 presents the computed values of e_w and estimated values of e (viz., caliper measurement). For estimation of 'e', the dry density, γ_d, was computed from the known weight of specimen and volume of specimen (average of five measurements) obtained by caliper measurement. The void ratio was estimated from the volume-mass relationship ($\gamma_d = G.\gamma_w$ / (1+e), where γ_w is the density of water. From Table 4, it can be observed that for intact specimens, $e_w \geq e$ for specimens I1 and I2, which indicates that the specimens are saturated at this stage. The values of e_w exceeding e may be attributed to experimental error associated with estimation of e. Fig. 4 suggests progressive shrinkage of both the size and volume of intra- and inter- aggregate pores during drying from specimen I1 to I2. However, the figure also depicts the presence of inter-aggregate pores with dominant size of about 30 μm (which can resist a capillary suction of just about 100 kPa) for specimen I2 (with total suction of 1.25 MPa), which would suggest desaturation of this specimen. However, the water retention characteristics as well as interpretation of MIP results confirm saturated state of specimen I2 and indicates the beginning of desaturation at a drying stage between specimens I2 and I3). This could be partially attributed to the dynamic process of simultaneous desaturation and shrinkage of pores, which

would cause time lag in the desaturation process and also delay complete desaturation of the pore. The shrinkage of pores results in equivalent reduction in volume of pores corresponding to the spillage of water during drying and increases the capillary suction required to remove water from the pore of reduced size, and this phenomena would result in pores remaining saturated. In addition to this, it is opined that the possible presence of saturated hidden larger pores trailing the smaller pores during drying process, might also contribute in preventing the desaturation of specimen I2. However, these larger pores would have been made accessible to intrusion of mercury during MIP tests, due to micro-cracking of soil specimen either during freeze drying process or during the air drying process itself. Further, for specimens I3 and I4, $e_w<e$, which indicates that some pores are unsaturated. For reconstituted specimens, R1, R2 and R3 it can be observed that $e_w \geq e$, indicating saturated pores for these specimens, whereas for specimen R4, $e_w<e$, which indicates that some pores are unsaturated. For compacted specimens prior to air drying viz., C21P1 and C25P1, $e_w \sim e$, which indicates that the pores are mostly saturated. However, for air dry specimens C21P2 and C25P2, $e_w<e$, suggests that the pores are partially saturated. In order to further distinguish the saturated pores from unsaturated pores, the computed e_w have been marked on the cumulative pore size distribution, as depicted in Figs. 3, 5 and 7.

Tarantino (2011) suggested that the intersection of e_w on the cumulative voids ratio curve indicates the demarcation of saturated and un-saturated pores. The pores smaller than this separation pore size (at point of intersection between e_w and cumulative voids ratio curve) can be assumed to be saturated and the pores larger than the separation pore size can be considered as un-saturated (the difference between e and e_w corresponds to the dry state of pores, and it is usually assumed that larger pores would de-saturate first). However, for soils with complex pore-

size distribution such as for swelling clay in this study, it would be difficult to conclude if only larger pores control the desaturation process.

For compacted specimens, as depicted in Fig. 7, the specimens C21P1 and C25P1 (initial state of compacted specimens) have mostly saturated pores ($e_w \sim e$). For specimen C21P1, during drying, both the inter-aggregate (some part) and intra-aggregate pores shrink. Some part of the inter-aggregate pores would have de-saturated and could not shrink further, represented by the final inter-aggregate pore volume for specimen C21P2. For specimen C25P1, it appears from Fig. 8 that the inter-aggregate pores de-saturate during drying, whereas the intra-aggregate pores shrink and try to remain saturated. At the end of air drying, intra-aggregate pores smaller than 0.036 μm and 0.055 μm (refer Fig. 8) appears to be still saturated for specimens C21P2 and C25P2, respectively, whereas the larger pores are de-saturated. It has been observed that the shrinkage during drying is higher for C25P1 as compared to C21P1, which may be attributed to higher initial water content for specimen C25P1 as compared to C21P1.

Further, for specimens C21P1 and C25P1, it can be seen (refer Table 2 and Fig. 8) that most of the shrinkage can be attributed to reduction in intra-aggregate pores. Li and Zhang (2009) have obtained similar inferences for compacted soil, where they observed that the mechanical compaction process results in reduction of inter-aggregate pores, whereas the hydraulic process of evaporation during drying results in reduction of mostly intra-aggregate pores. This indicates the role of mechanical and hydraulic processes in altering the pore structure of the compacted samples during compaction process and drying, respectively.

Discussion

The conventional capillary model for explaining the drying process, suggests that pores would de-saturate if the suction exceeds the capillary pressure represented by Young-Laplace equation (refer Eqn. 4).

$$\psi = \frac{4.T.\cos(\alpha)}{d} \qquad (4)$$

where ψ is the suction due to capillary forces in MPa, T is the interfacial tension at air-water-solid interface = 0.072 N/m, α is the contact angle, d is the pore diameter in μm.

Usually the contact angle, α, is assumed to be zero during drying process (Marshall et al. 1996), which would yield maximum capillary pressure that can be sustained by the pores, before de-saturating (represented by Eqn. 5).

$$\psi = \frac{4.T}{d} \qquad (5)$$

Interestingly, the microstructural evolution of the swelling clay SC1 in this study, which exhibits shrinkage of the pores during the drying process, suggests the deformable nature of the pores. Hence, at each stage of drying, when the suction equalizes the capillary pressure which can be sustained by the pores of certain size, these pores spill some water and in the process shrink. Hence, these pores of reduced size can now sustain higher capillary pressure, and are still saturated. When suction increases during the drying process and equalizes this new capillary pressure sustained by the pores, more water spills from the pores and the pores shrink further and manage to resist higher capillary pressure preventing remaining water from spilling from the pores. This process may continue till the pores can shrink further. During the process of drying, some pores would de-saturate and would not undergo further shrinkage (larger group of pores for specimen R4; inter-aggregate pores for specimens I3, I4, C21P2 and C25P2 and part of intra-

aggregate pores for specimens C21P2 and C25P2), whereas other pores would undergo shrinkage and would be still saturated (most of the pores for specimens I2, R2, R3; most of the intra-aggregate pores for specimens I3, and part of intra-aggregate pores for specimens C21P2 and C25P2). For such clays, which exhibit substantial shrinkage, the suction-pore size relationship may appropriately be represented by Eqn. 5 only if the diameter d is assumed to evolve during the drying process. It is opined that a model which incorporates the deformable capillary tube effect, to represent the shrinkage of pores during drying, might be able to explain the evolution of pore structure and the de-saturation process, during drying, for such swelling clays (viz., soil SC1).

In order to confirm this hypothesis for the swelling clay, the theoretical maximum pore-diameter, d, for a saturated pore has been computed corresponding to different values of matric suction, ψ_m for the intact, reconstituted and compacted specimens, using Eqn. 5. The theoretical maximum pore-diameter, d, has been compared with the actual experimental values of dominant pore diameter, d_d (the diameter corresponding to peak of frequency pore size distribution curve, refer Figs. 4,6 and 8), and also the entrance pore diameter, d_e (largest pore diameter which would probably permit the entry of air into the specimen at the onset of desaturation, which can be obtained from the frequency pore size distribution curve, as the largest pore diameter at which mercury intrusion into intra-aggregate pores begins) for the intact, reconstituted and compacted specimens at different stages of drying. It should be noted that the concept of entrance pore diameter, d_e, is introduced in this study to quantify the capillary suction corresponding to beginning of desaturation of pores. Fig. 10 depicts the methodology for obtaining the value of d_e from a typical cumulative pore size distribution curve. The point at which the slope of the cumulative pore size distribution curve changes, defines d_e.

It should be noted that Laplace equation relates matric suction, ψ_m with the pore diameter, d, whereas total suction, ψ, is obtained from the experimental studies. Hence, in order to compare the experimental results with the Laplace equation, an attempt has been made to estimate the osmotic suction, ψ_o, in order to convert the experimentally obtained ψ to ψ_m (matric suction). The model proposed by Peroni and Tarantino (2004) is considered for estimation of ψ_o, as represented by Eqn. 6.

$$\psi_o = \frac{A}{(w-B)} \tag{6}$$

where A and B are fitting parameters

In the model, the parameter B which is equal to the hygroscopic water content, $w_{adsorbed}$ is considered as 0.07 and the parameter A has been fitted for the osmotic suction, ψ_o, associated with the specimen at $w = 5$ (osmotic suction, ψ_o is inferred from electrical conductivity, EC, measurement on pore solution as per Eqn. 7, suggested by USDA 1950 (Peroni and Tarantino, 2004). The parameter A is obtained as 112.3 corresponding to $\psi_o = 22.78$ kPa (EC= 732 μS/cm).

$$\psi_o = 0.0191\, EC^{1.074} \tag{7}$$

The relationship between osmotic suction, ψ_o vs water content, w, computed based on Peroni and Tarantino (2004) model is depicted in Fig. 11. The estimation of experimental values of matric suction, ψ_m, for intact, reconstituted and compacted specimens, as per Eqn. 8, is summarized in Table 5.

$$\psi_m = \psi - \psi_o \tag{8}$$

The theoretical relationship of matric suction, ψ_m vs pore diameter, d based on Laplace equation (Eqn. 5) has been plotted as depicted in Figs. 12 and 14 (depicted as $T_{Laplace}$). Further, the figures also depict the experimental relationship of ψ_m vs d_d and ψ_m vs d_e (refer Fig. 12 for

intact and reconstituted specimens and Fig. 14 for compacted specimens). In the Figs. 12 and 14, suffixes 'Actual-d' and 'Actual-e' corresponds to experimental values of ψ_m, with respect to dominant pore diameter, d_d, and entrance pore-diameter, d_e, respectively.

For the reconstituted specimens, the superimposition of experimental values of ψ_m–entrance pore diameter vs d_e relationship in Fig. 12 ('Actual-e' in figure), suggests that the ψ_m vs d_e data lies on the Laplace curve for the specimens R1 and R2, which indicates that these specimens are saturated due to progressive shrinkage of the specimens during drying. The capillary forces with which water is held in the pores are higher enough to resist the developed suction and hence prevents the desaturation of the pores. Moreover, it appears that the larger pores adjust their size to prevent desaturation (as the data points for R1 and R2 move along the Laplace curve). Further, it can be observed from the figure that the ψ_m vs d_e data detaches from the Laplace curve for specimens R3 and R4, which indicates that these specimens are partially saturated (suction is higher than the capillary suction represented by Laplace equation, and the specimens starts desaturating due to the fact that the largest pores cannot sustain the developed suction). Further, the superimposition of ψ_m–dominant pore diameter, d_d ('Actual-d' in figure) relationship in Fig. 12 suggests most of the intra-aggregate (micro) pores of the specimen R3 are also saturated, as ψ_m–d_d relationship lies below the Laplace curve. Further for specimen R4 it can be also noted that the ψ_m–d_d relationship lies above the Laplace curve, which indicates desaturation of micro-pores for R4. This is consistent with Fig.5, which shows that micro-pores in specimens R1, R2 and R3 are saturated, whereas micro-pores in R4 are partially saturated.

For the intact specimens, the superimposition of experimental values of ψ_m–entrance pore diameter, d_e ('Actual-e' in figure) relationship in Fig. 12, suggests that the ψ_m vs d_e data lies below the Laplace curve for the specimens I1 and I2, which indicates that these specimens are

saturated. Further, it can be observed from the figure that the ψ_m vs d_e data lies above the Laplace curve for specimens I3 and I4, which indicates that these specimens are partially saturated (suction is higher than the capillary suction represented by Laplace equation). This is consistent with Fig. 3, which shows that specimens I1 and I2 are saturated, whereas I3 and I4 are partially saturated. Further, the superimposition of ψ_m–dominant pore diameter, d_d ('Actual-d' in figure) relationship in Fig. 12 suggests most of the intra-aggregate (micro) pores of the specimens I3 are also saturated, whereas the ψ_m–d_d relationship for specimen I4 is above the Laplace curve indicating significant desaturation of micro-pores for specimen I4 during further drying as compared to I3.

It should be noted that for intact specimens, the larger inter-aggregate pores (viz., macropores) form significant fraction of the total porosity of the specimen (about 25% for specimen I1 and 20% for specimen I2). These pores are quite large and would desaturate at low suction values, which is in contrast with the experimental data which indicate these specimens to be saturated. This contrast may be explained by the mechanism depicted in Fig. 13.

As depicted in Fig. 13, d_{1a}, d_{1b} and d_{1c} are diameter of larger pore at different stages of drying; T_{1a}, T_{1b} and T_{1c} are air-water interface tension (capillary suction) in larger pore at different stages of drying; d_{2a}, d_{2b} and d_{2c} are diameter of smaller pore at different stages during desaturation; T_{2a} is capillary suction in smaller pore at desaturation of larger pore. At initial stage of drying from saturated state, as depicted in Fig. 13 (a), the air-water-interface tension is T_{1a} in larger pore of diameter d_{1a}. The diameter of smaller pore is d_{2a}. During drying, the air-water interface tension in larger pore increases to T_{1b} and the larger pore shrinks by equivalent volume and reduces to new diameter, d_{1b} and the smaller pore undergoes no change (refer Fig. 13b). With further drying, the air-water interface recedes into the larger pore due to the evaporation of

water from the surface, and the interface tension reaches its maximum value, T_{1c}. During the transient process, however, the larger pore will eventually empty experiencing shrinkage to residual diameter, d_{1c}. The smaller pore acts as water channel and loses water to upper pore and shrinks to new diameter, d_{2b} (refer Fig. 13c). At this stage, the larger pore has desaturated and reduced to residual diameter, d_{1c}. The air-water interface recedes into the smaller pore with interface tension, $T_{2a} > T_{1c}$. By this time the smaller pore has shrunk to new diameter d_{2c}. The desaturation process of smaller pore continues as explained in Steps above (refer Fig. 13d). Similar mechanism as explained in Fig. 13 may also occur with larger pore trailing the smaller pore at the surface, and the desaturation of the larger pore may occur only after the desaturation process of the upper (leading) smaller pore is completed.

The above mechanism can be understood for specimen I2, which has inter-aggregate porosity (viz., macro-pores) of about 20%, and would have degree of saturation, S about 80%. However, these macro-pores are likely to be the pores surrounded by smaller pores and hence hidden by these saturated smaller pores during the drying process. These hidden larger macro-pores are probably accessed by the mercury during MIP tests (refer Fig. 3), due to possible micro-cracks formed during freeze drying or the air drying process. The shrinkage of macro-pores for specimen I3 as compared to specimen I2 (refer Fig. 4) is associated with the mechanism depicted in Fig. 13.

For the compacted specimens C21P1 and C25P1, Fig. 14 depicts that ψ_m vs d_e ('Actual-e') relationship lies above the Laplace curve, indicating that the entrance micro-pores are desaturated. However, the superimposition of ψ_m vs d_d ('Actual-d') relationship in Fig. 14 suggests that most of the micro-pores of specimens C21P1 and C25P1 are saturated, as ψ_m vs d_d relationship is below the Laplace curve. However, for air dry specimens C21P2 and C25P2, both

the ψ_m vs d_e and ψ_m vs d_d relationships are above the Laplace curve, which indicates that most of the micro-pores of the compacted specimens in air dry state are desaturated. These observations are consistent with the interpretation from Fig. 7 that the micro-pores for specimens C21P1 and C25P1 are saturated and subsequently get desaturated at higher suction during drying. It may be noted that the inter-aggregate (macro) pores of specimens C21P1 and C25P1 are expected to desaturate at lower suction during beginning of the drying process. This can be confirmed from the fact the macro-pores exhibit negligible shrinkage during drying (refer Fig. 7). Hence, it can be seen that the water retention behaviour of swelling clays can be understood by Laplace model for capillary suction, wherein the pore size evolves during the drying process. Further, the swelling clays exhibit progressive shrinkage during drying, and during this process the desaturation of pores experiences delay as explained in Fig. 13.

Fig. 15 depicts the d-ψ_m relationship for a hypothetical non-deformable capillary tube (viz., pores), hypothetical deformable capillary tube and Laplace curve (viz., theoretical d-ψ_m relationship based on equation Eqn. 5). The point, where the d-ψ_m relationship for non-deformable capillary tube crosses the Laplace curve, indicates the point of desaturation of non-deformable pores. At this point, the suction in the largest pore accessible to air entry is larger than the capillary pressure that can be sustained by these pores. These pores do not undergo shrinkage as they desaturate.

For deformable pores, when the suction reaches the capillary pressure that can be sustained by the pores, part of the water spills off the pores, and simultaneously the pores shrink to develop higher capillary pressure and shrinkage equal to the volume of the spilled water occurs. The new pores of reduced size can sustain the suction developed and remain saturated. This process continues till these pores can shrink and the capillary pressure is higher than the

suction developed, and the desaturation process starts only when the largest pores accessible to

entry of air cannot shrink further. Fig. 15 also depicts the point, where the d-ψ_m relationship for

deformable capillary tube crosses the Laplace curve, which indicates their point of desaturation.

The deformable capillary tube concept is quite valid for the intact and reconstituted specimens of

the swelling clay, which exhibit shrinkage for most part of drying.

The comparison of microstructural evolution of the soil during drying from undisturbed

and reconstituted states, suggest that the pore-size distribution during dry end is quite similar for

both intact and reconstituted specimens (refer Tables 2 and 3). Based on these inferences, and the

discussion related to SWRCs of these clays, it can be opined that the deformability (shrinkage) of

the pores during drying process results into convergence of the pore-size distribution of the

swelling clay in intact and reconstituted states, after a stage of drying. However, generalization

of this hypothesis requires extensive studies on other swelling clays.

Conclusions

The present study attempts to understand the water retention behaviour and

microstructure of swelling clay dried from initial intact, reconstituted and compacted states. The

following conclusions can be drawn from the study:

1. It has been noted that the drying-path SWRCs for the swelling clay studied from the intact

    and reconstituted states, converge beyond a critical suction value. The drying path SWRCs of

    the clays in their compacted state exhibit lower suction at particular water content as

    compared to the intact and reconstituted states.

2. Based on the study, it can be opined that both the inter-aggregate and intra-aggregate pores influence the water retention behaviour of the compacted clays. This observation is in line with findings of earlier studies.

3. For swelling clay (viz., soil SC1) it is observed that the specimens in the intact and compacted states exhibit bimodal pore-size distribution during drying path, whereas the specimens in reconstituted state exhibit mono-modal pore-size distribution.

4. The pore-size distribution for swelling clay (viz., soil SC1) in relatively dry state (viz., beyond critical suction, ψ_c) is quite similar for both intact and reconstituted specimens, which may be attributed to shrinkage of pores to residual pore size distribution during drying. However, generalization of this hypothesis requires more studies on other swelling soils.

5. The concept of entrance pore diameter, d_e has been introduced in the study to explain the desaturation process of intact, reconstituted and compacted specimens of swelling clay.

6. The study observes the progressive deformation of the pores during drying for the intact and reconstituted specimens of swelling clay, which suggests the applicability of Laplace equation in general for swelling clays.

Acknowledgement

References

Agus, S. S., Schanz, T., 2006. Drying, wetting and suction characteristics curve of bentonite-sand mixture. Proceedings of 4th international conference on Unsaturated Soils, Carefree, AZ, Geotechnical Special Publication No. 147, 1405-1414.

Ahmed, S., Lovell, C.W. Jr., Diamond, S., 1974. Pore size and strength of compacted clay. Journal of the Geotechnical Engineering Division, ASCE, 100 (4), 407–425.

Arnepalli, D. N., Shanthakumar. S., Rao, B. H., Singh, D. N., 2008. Comparison of methods for determining specific-surface area of fine-grained soils, Geotechnical and Geological Engineering, 26, 121-132.

ASTM D 2487-06e1, 2006. Standard Practice for Classification of Soils for Engineering Purposes (Unified Soil Classification System), Annual Book of ASTM Standards, ASTM International, West Conshohocken, PA.

ASTM D 422, 1994. Standard Test Method for Particle Size Analysis of Soils, Annual Book of ASTM Standards, ASTM International, West Conshohocken, PA.

ASTM D 427-98, 2004. Standard Test Method for Shrinkage Factors of Soils by the Mercury Displacement Method, In Annual Book of ASTM Standards, American Society for Testing and Material, ASTM International, Philadelphia, Pa.

ASTM D 4318, 2005. Standard Test Methods for Liquid Limit, Plastic Limit, and Plasticity Index of Soil, Annual Book of ASTM Standards, ASTM International, West Conshohocken, PA.

ASTM D 5550, 2006. Standard Test Method for Specific Gravity of Soil Solids by Gas Pycnometer, Annual Book of ASTM Standards, ASTM International, West Conshohocken, PA.

Burton, G. J., Pineda, J. A., Sheng, D. and Airey, D. 2015. Microstructural changes of an undisturbed, reconstituted and compacted high plasticity clay subjected to wetting and drying. Engineering Geology, 193, 363-373.

Charles, W. W. Ng., Pang, Y. W., 2000a. Influence of stress state on soil-water characteristic and slope stability. Journal of Geotechnical and Geoenvironmental. Engineering, 126(2), 157-166.

Charles, W. W. Ng., Pang, Y. W., 2000b. Experimental investigations of the soil-water characteristics of a volcanic soil. Canadian Geotechnical Journal, 37, 1252-1264.

Cuisinier, O., Laloui, L., 2004. Fabric evolution during hydromecanical loading of a compacted silt. International Journal of Numerical and Analytical Methods in Geomechanics, 28(6), 483–499.

Decagon Devices Inc., 2010. WP4C Operator Manual. Decagon Devices Inc., United States of America.

Delage, P., 2009. Discussion: Compaction behaviour of clay, Géotechnique, 59(1), 75–77.

Delage, P., Lefebvre, G., 1984. Study of the structure of a sensitive Champlain clay and of its evolution during consolidation. Canadian Geotechnical Journal, 21, 21-35.

Delage, P., Audiguier, M., Cui, Y.J., Howat, M.D., 1996. Microstructure of a compacted silt. Canadian Geotechnical Journal, 33, 150–158.

Diamond, S. 1971. Microstructure and pore structure of impact-compacted clays. Clays and Clay Minerals, 19, 239-249.

Dieudonne, A. C., Vecchia, G. D., Charlier, R., Jommi, C., 2014. Influence of microfabric evolution on the retention behaviour of compacted clayey soils. Proceedings of 6th International Conference on Unsaturated Soils, UNSAT 2014, Sydney, Australia, 679-684.

Djeran-Maigre., Tessier, D., Grunberger, D., Velde, B. and Vasseur, G. 1998. Evolution of microstructures and of macroscopic properties of some clays during experimental compaction. Marine and Petroleum Geology, 15, 109-128.

Fredlund, D. G., Sheng, D., Zhao, J., 2011. Estmation of soil suction from the soil-water characteristic curve. Canadian Geotechnical Journal, 48, 186-198.

Fredlund, M. D., Wilson, G. W., Fredlund, D. G., 2002. Use of grain size distribution curve for estimation of the soil water characteristics curve. Canadian Geotechnical Journal, 39, 1103-1117.

Frydman, S., Baker, R., 2009. Theoretical Soil-Water Characteristic Curves Based on Adsorption, Cavitation, and a Double Porosity Model. International Journal of Geomechanics, 9(6), 250-257.

Garcia-Bengochea, I., Lovell, C.W., Altschaeffl, A.G., 1979. Pore distribution and permeability of silty clays. Journal of the Geotechnical Engineering Division, ASCE, 105(7), 839–856.

Gens, A., Alonso, E.E., Suriol, J., Lloret, A., 1995. Effect of structure on the volumetric behaviour of a compacted soil. Proc. 1st Int. Conf. on Unsaturated Soils, Paris Vol. 1, 83–88.

Gumaste, S.D., Iyer, K.R., Sharma, S., Singh, D.N. 2014a. Determination of the fabric alteration of marine clays. Acta Geotechnica Slovenica, 11(2), 21-31.

Gumaste, S.D., Iyer, K.R., Sharma, S., Channabasavaraj, W., Singh, D.N., 2014b. Simulation of fabric in sedimented clays. Applied Clay Science, 91-92, 117-126.

Hattab, M., Hammad, T., Fleureau, J. M., Hicher, P. Y., 2013. Behaviour of a sensitive marine sediment: microstructural investigation. Géotechnique, 63(1), 71–84.

IS 2720-Part XL, 2002. Determination of free swell index of soils. Bureau of Indian Standard, New Delhi.

Iyer, K. R., Jayanth, S., Gurnani, S., Singh, D.N., 2013. Influence of Initial Water Content and Specimen Thickness on the SWCC of Fine-grained Soils. International Journal of Geomechanics, ASCE, 13(6), 894-899.

Jayanth, S., Iyer. K., Singh, D. N., 2012. Influence of drying and wetting cycles on SWCCs of fine-grained soils. Journal of Testing and Evaluation, ASTM, 40(3), 376-386.

Kawai, K., Karube, D., Kato, S., 2000. The model of water retention curve considering effects of void ratio. Proc. Asian Conf. on Unsaturated Soils, Singapore, 329-334.

Kolay, P. K., Singh, D. N., 2000. Effect of Zeolitization on compaction, consolidation and permeation characteristics of a lagoon ash. Journal of Testing and Evaluation, ASTM, 28(6), 425-430.

Konyai, S., Sriboonlue, V., Treloges, V., Muangson, N., 2006. Hysteresis of water retention curve of saline soil. Proceedings of 4th international conference on unsaturated soils, Carefree, Arizona, 1394-1404.

Li, X., Zhang, L. M., 2009. Characterization of dual-structure pore-size distribution of soil. Canadian Geotechnical Journal, 46, 129-141.

Likos, W. J., Lu, N., 2002. Hysteresis of capillary cohesion in unsaturated soils. 15th ASCE Engineering Mechanics Conference, Columbia University, New York, USA.

Lopes, B.C.F.L., Tarantino, A., Cordão-Neto, M.P., 2014. An approach to detect micro- and macro-porosity from MIP data. Proceedings of 6th International Conference on Unsaturated Soils, UNSAT 2014, Sydney, Australia, 685-690.

Marinho, F. A. M., 2005. Nature of soil-water characteristic curve for plastic soils. Journal of Geotechnical and Geoenvironmental Engineering, 131(5), 654-661.

Marshall, T. J., Holmes, J. W., and Rose, C. W., 1996. Soil Physics. Cambridge University Press, Cambridge, UK.

Miller, C. J., Yesiller, N., Yaldo, K., Merayyan, S., 2002. Impact of soil type and compaction conditions on soil water characteristic. Journal of Geotechnical and Geoenvironmental Engineering, 128(9), 733-742.

Mohamed, M., H., A., Sharma, R., S., 2007. Role of dynamic flow in relationships between suction head and degree of saturation. Journal of Geotechnical and Geoenvironmental Engineering,133 (3), 286-294.

Monroy, R., Zdravkovic, L. and Ridley, A. 2010. Evolution of microstructure in compacted London clay during wetting and loading. Geotechnique, 60(2), 105-119.

Ninjgarav, E., Chung, S.-G., Jang, W.-Y., Ryu, C-K., 2007. Pore Size Distribution of Pusan Clay Measured by Mercury Intrusion Porosimetry. KSCE Journal of Civil Engineering, 11(3), 133–139.

Noh, J. H., Lee, S. R., Park, H., 2011. Prediction of cryo-SWCC during freezing based on pore size distribution. International Journal of Geomechanics, 12(4), 428-438.

Pham, H. Q., Fredlund, D. G., 2008. Equations for the entire soil-water characteristic curve of a volume change soil. Canadian Geotechnical Journal, 45, 443-453.

Pham, H. Q., Fredlund, D. G., Barbour, S. L., 2005. A study of hysteresis models for soil water characteristic curves. Canadian Geotechnical Journal, 42, 1548-1568.

Peroni, N., Tarantino, A., 2004. Measurement of osmotic suction using the squeezing technique. Unsaturated soils: Experimental Studies, T. Schanz (ed.), Proceedings of International

Conference 'From Experimental Evidence towards Numerical Modelling of Unsaturated Soils', Weimar, Germany, 159-168.

Prapaharan, S., White, D.M., Altschaeffl, A.G., 1991. Fabric of field- and laboratory-compacted clay. Journal of Geotechnicla Engineering, ASCE, 117(12), 1934–1940.

Ridley, A. M., Romero, J. P., 1998. Suction-water content relationships for a range of compacted soils. Proceedings of The Second International Conference on Unsaturated Soils, Beijing, China, 114-118.

Romero, E., Della Vecchia, D., Jommi, C., 2011. An insight into the water retention properties of compacted clayey soils. Geotechnique, 61(4), 313-328.

Romero, E., Gens, A., Lloret, A., 1999. Water permeability, water retention and microstructure of unsaturated compacted Boom clay. Engineering Geology, 54, 117–127.

Seiphoori, A., Ferrari, A. and Laloui, L. 2014. Water retention behaviour and microstructural evolution of MX-80 bentonite during wetting and drying cycles. Geotechnique, 64(9), 721-734.

Simms P.H., Yanful, E.K., 2001. Measurement and estimation of pore shrinkage and pore distribution in a clayey till during soil-water characteristic curve tests. Canadian Geotechnical Journal, 38, 741–754.

Souli, H., Fleureau, M., Trabelsi, A.M., Besnard, M., 2008. Physicochemical analysis of permeability changes in the presence of zinc. Geoderma, 145(1-2), 1-7.

Sreedeep, S., Singh, D. N., 2005. A study to investigate the influence of soil properties on suction. Journal of Testing and Evaluation, ASTM, 33(1), 1-6.

Sridharan, A., Altschaeffl, A.G., Diamond, S., 1971. Pore size distribution studies. Journal of Soil Mechanics and Foundation Division, ASCE, 97, 771–787.

Tanaka, H., Shiwakoti, D.R., Omukai N., Rito F., Locat J., Tanaka M., 2003. Pore size distribution of clayey soils measured by mercury intrusion porosimetry and its relation to hydraulic conductivity. Soils and Foundations, 43(6), 63–67.

Tarantino, A., De Col, S., 2008. Compaction behaviour of clay. Geotechnique, 58 (3), 199–213.

Tarantino, A., 2011. Unsaturated soils: Compacted versus reconstituted states. 5th International Conference on Unsaturated Soil, Barcelona, Spain, 113-136.

Thakur, V. K. S., Sreedeep, S., Singh, D. N., 2005. Parameters affecting soil–water characteristic curves of fine-grained soils. Journal of Geotechnical and Geoenvironmental Engineering, 131(4), 521-524.

Thakur, V. K. S., Sreedeep, S., Singh, D. N., 2006. Laboratory investigations on extremely high suction measurements for fine-grained soils. Journal of Geotechnical and Geological Engineering, 24, 565-578.

Tinjum, J. M., Benson, C. H., Blotz, L. R., 1997. Soil-water characteristic curve of compacted clays. Journal of Geotechnical and Geoenvironmental Engineering, 123(11), 1060-1069.

Tuller, M., Or, Dani., 2005. Water films and scaling of soil characteristic curves at low water contents. Water Resources Research, 41, 1-6.

Vanapalli, S. K., Pufahl, D. E., Fredlund, D. G., 1998. The effect of stress state on the soil-water characteristic behaviour of a compacted sandy-clay till. Proceedings of 51st Canadian Geotechnical Conference, 81-86.

Vanapalli, S. K., Pufahl, D. E., Fredlund, D. G., 1999. The effect of soil structure and stress history on the soil-water characteristics ofa compacted till. Geotechnique, 49(2), 143-159.

Yang, H., Rahardjo, H., Leong, C., Fredlund, D. G., 2004. Factors affecting drying and wetting soil-water characteristic curves of sandy soils. Canadian Geotechnical Journal, 41, 908-920.

Geomechanics and Geoengineering: An International Journal

Table 1 Physical and mineralogical characteristics of the swelling clay SC1

Clay	G	Particle size distribution (%)			Atterberg Limits (%)					FSI (%)	SSA m^2/g	USCS	Major Minerals
		Sand	Silt	Clay	w_l	w_p	I_p	w_s	I_s				
SC1	2.62	5	25	70	114	22	92	16	06	130*	303	CH	Quartz, Montmorillonite

*Colloidal suspension observed

Table 2. Summary of the MIP results for intact & compacted specimens of swelling clay SC1 based on the modified van Genuchten dual porosity model

Specimen	$^*d_{d1}$ (μm)	$^*d_{d1avg}$ (μm)	$^*d_{d2}$ (μm)	$^*d_{d2avg}$ (μm)	Intra-aggregate pore		Inter-aggregate pore	
					(%)	$^{**}e_m$	(%)	$^{**}e_M$
I1	0.018-0.026	0.022	21.44-44.33	32.89	64.80	0.432	35.20	0.235
I2	0.015-0.019	0.017	24.74-35.01	29.88	72.34	0.380	27.66	0.144
I3	0.012-0.016	0.014	20.11-37.44	28.78	80.88	0.380	19.12	0.090
I4	0.007-0.009	0.008	18.87-35.24	27.06	76.44	0.222	23.56	0.068
C21P1	0.017-0.027	0.022	10.84-20.37	15.61	73.06	0.325	26.94	0.120
C21P2	0.012-0.016	0.014	12.79-24.66	18.73	72.70	0.200	27.30	0.075
C25P1	0.024-0.032	0.028	31.22-49.44	40.33	72.88	0.280	27.12	0.100
C25P2	0.012-0.018	0.015	25.67-40.73	33.20	60.48	0.168	39.52	0.110

$^*d_{d1}$ =Dominant pore diameter (intra-aggregate pores as per van Genuchten dual porosity model)
$^*d_{d2}$ =Dominant pore diameter (inter-aggregate pores as per van Genuchten dual porosity model)
$^{**}e_m$ = voids ratio of intra-aggregate pores from MIP results
$^{**}e_M$ = voids ratio of inter-aggregate pores from MIP results

Table 3. Summary of the MIP results for reconstituted specimens of swelling clay SC1 based on the modified van Genuchten porosity model (mono-modal)

Specimen	$^*d_d$ (μm)	$^*d_{davg}$ (μm)	$^{**}e_{MIP}$
R1	4.10	4.10	2.65
R2	0.080-0.103	0.092	0.79
R3	0.007-0.011	0.009	0.34
R4	0.006-0.008	0.007	0.24

$^*d_d$ =Dominant pore diameter

$^{**}e_{MIP}$ =voids ratio from MIP results

Table 4 Comparison of the e_w and e at different stages of drying for different specimens of the swelling clay SC1

Specimen	e_w	e
I1	1.10	1.03
I2	0.99	0.93
I3	0.57	0.66
I4	0.37	0.48
R1	3.20	3.11
R2	1.21	1.15
R3	0.68	0.64
R4	0.33	0.41
C21P1	0.54	0.56
C21P2	0.24	0.37
C25P1	0.66	0.65
C25P2	0.26	0.40

Table 5 Estimation of matric suction, ψ_m for different specimens of the swelling clay SC1 based on Peroni and Tarantino (2004) model for osmotic suction

Specimen	w (g/g)	ψ MPa	ψ_o MPa	$\psi_m = \psi - \psi_o$ MPa
I1	0.420	0.07	0.06	0.01
I2	0.379	1.52	0.36	1.16
I3	0.233	12.71	0.69	12.02
I4	0.147	66.96	1.53	65.43
R1	1.157	0.13	0.10	0.03
R2	0.458	1.25	0.29	0.96
R3	0.259	13.11	0.60	12.51
R4	0.131	62.50	1.84	60.66
C21P1	0.210	6.77	0.80	5.97
C21P2	0.100	62.10	3.74	58.36
C25P1	0.250	4.09	0.62	3.47
C25P2	0.092	51.02	5.10	45.92

List of Figure Captions

Fig. 1   Comparison of the drying- path SWRCs for the swelling clay used in this study

Fig. 2   Details of the specimens selected for the micro-structure analysis

Fig. 3   Pore size distribution with respect to cumulative voids ratio for swelling clay SC1-Intact state

Fig. 4   Pore size distribution with respect to incremental voids ratio for swelling clay SC1-Intact state

Fig. 5   Pore size distribution with respect to cumulative voids ratio for swelling clay SC1-Reconstituted state

Fig. 6   Pore size distribution with respect to incremental voids ratio for swelling clay SC1-Reconstituted state

Fig. 7   Pore size distribution with respect to cumulative voids ratio for swelling clay SC1-Compacted state

Fig. 8   Pore size distribution with respect to incremental voids ratio for swelling clay SC1-Compacted state

Fig. 9   Fitting of cumulative voids ratio with modified van Genuchten equation for specimens I3 and R3

Fig. 10   Methodology for determining entrance pore diameter, d_e, from cumulative pore-size distribution

Fig. 11   Relationship between osmotic suction, ψ_o and water content, w, based on Peroni and Tarantino (2004) model

Fig. 12   Relationship between matric suction, ψ_m, and pore diameter, d, for the Intact and Reconstituted specimens of the swelling clay SC1

Fig. 13   Mechanism of desaturation and shrinkage in Swelling Clays

Fig. 14   Relationship between matric suction, ψ_m, and pore diameter, d, for Compacted specimens of swelling clay SC1

Fig. 15   Deformable capillary tube concept

1
2
3
4
5
6
7
8
9
10
11
12
13
14
15
16
17
18
19
20
21
22
23
24
25
26
27
28
29
30
31
32
33
34
35
36
37
38
39
40
41
42
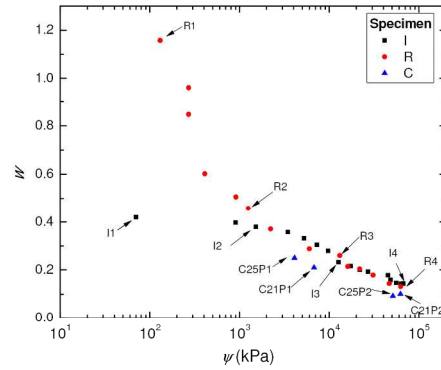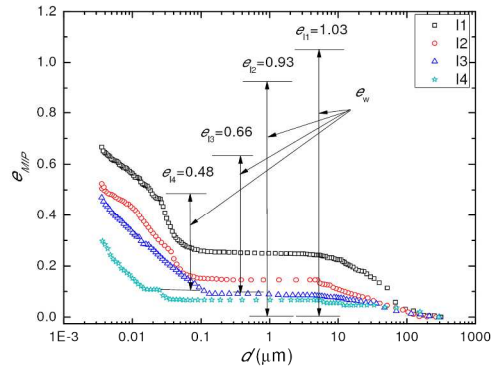43
44
45
46
47
48
49
50
51
52
53
54
55
56
57
58
59
60

Fig. 1

Comparison of the drying- path SWRCs for the swelling clay used in this study

215x279mm (290 x 290 DPI)

1
2
3
4
5
6
7
8
9
10
11
12
13
14
15
16
17
18
19
20
21
22
23
24
25
26
27
28
29
30
31
32
33
34
35
36
37
38
39
40
41
42
43
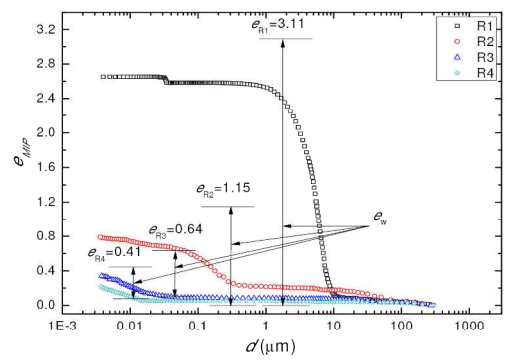44
45
46
47
48
49
50
51
52
53
54
55
56
57
58
59
60

Fig. 2

Details of the specimens selected for the micro-structure analysis

215x279mm (290 x 290 DPI)

1
2
3
4
5
6
7
8
9
10
11
12
13
14
15
16
17
18
19
20
21
22
23
24
25
26
27
28
29
30
31
32
33
34
35
36
37
38
39
40
41
42
43
44
45
46
47
48
49
50
51
52
53
54
55
56
57
58
59
60

Fig. 3

Pore size distribution with respect to cumulative voids ratio for swelling clay SC1-Intact state
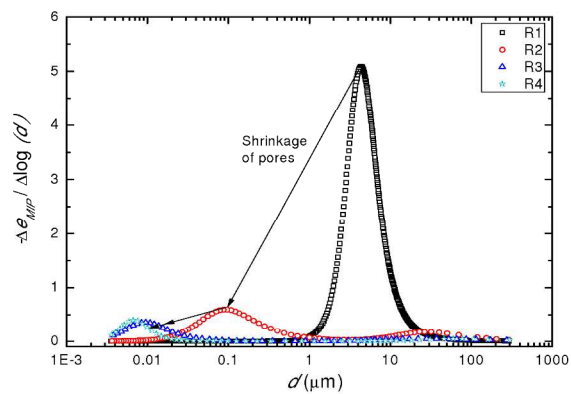
215x279mm (290 x 290 DPI)

1
2
3
4
5
6
7
8
9
10
11
12
13
14
15
16
17
18
19
20
21
22
23
24
25
26
27
28
29
30
31
32
33
34
35
36
37
38
39
40
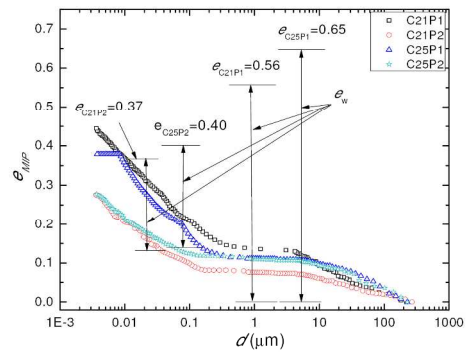41
42
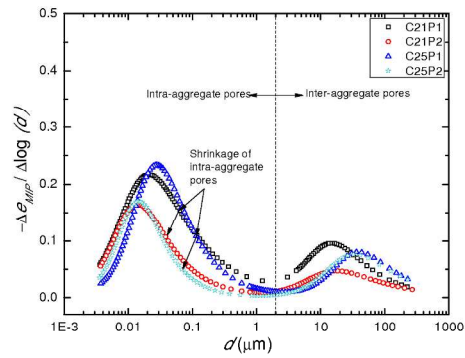43
44
45
46
47
48
49
50
51
52
53
54
55
56
57
58
59
60
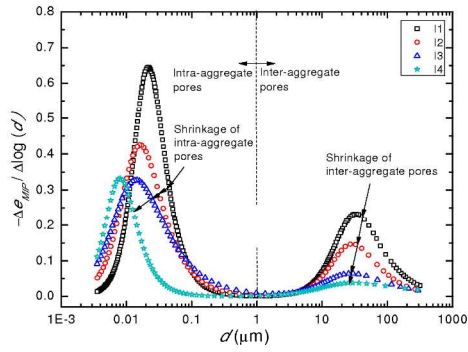
Fig. 4

Pore size distribution with respect to incremental voids ratio for swelling clay SC1-Intact state

215x279mm (290 x 290 DPI)

1
2
3
4
5
6
7
8
9
10
11
12
13
14
15
16
17
18
19
20
21
22
23
24
25
26
27
28
29
30
31
32
33
34
35
36
37
38
39
40
41
42
43
44
45
46
47
48
49
50
51
52
53
54
55
56
57
58
59
60

Fig. 5

Pore size distribution with respect to cumulative voids ratio for swelling clay SC1-Reconstituted state

215x279mm (290 x 290 DPI)

1
2
3
4
5
6
7
8
9
10
11
12
13
14
15
16
17
18
19
20
21
22
23
24
25
26
27
28
29
30
31
32
33
34
35
36
37
38
39
40
41
42
43
44
45
46
47
48
49
50
51
52
53
54
55
56
57
58
59
60

Fig. 6

Pore size distribution with respect to incremental voids ratio for swelling clay SC1-Reconstituted state

215x279mm (290 x 290 DPI)

1
2
3
4
5
6
7
8
9
10
11
12
13
14
15
16
17
18
19
20
21
22
23
24
25
26
27
28
29
30
31
32
33
34
35
36
37
38
39
40
41
42
43
44
45
46
47
48
49
50
51
52
53
54
55
56
57
58
59
60

Fig. 7

Pore size distribution with respect to cumulative voids ratio for swelling clay SC1-Compacted state

215x279mm (290 x 290 DPI)

Fig. 8

Pore size distribution with respect to incremental voids ratio for swelling clay SC1-Compacted state

215x279mm (290 x 290 DPI)

1
2
3
4
5
6
7
8
9
10
11
12
13
14
15
16
17
18
19
20
21
22
23
24
25
26
27
28
29
30
31
32
33
34
35
36
37
38
39
40
41
42
43
44
45
46
47
48
49
50
51
52
53
54
55
56
57
58
59
60
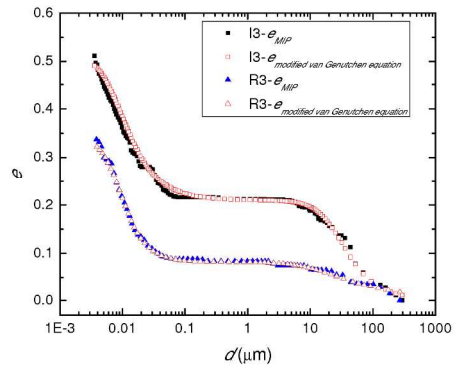
Fig. 9

Fitting of cumulative voids ratio with modified van Genuchten equation for specimens I3 and R3
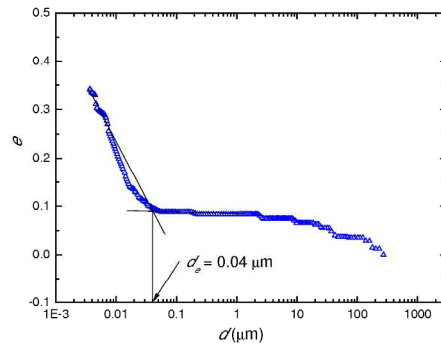
215x279mm (290 x 290 DPI)

1
2
3
4
5
6
7
8
9
10
11
12
13
14
15
16
17
18
19
20
21
22
23
24
25
26
27
28
29
30
31
32
33
34
35
36
37
38
39
40
41
42
43
44
45
46
47
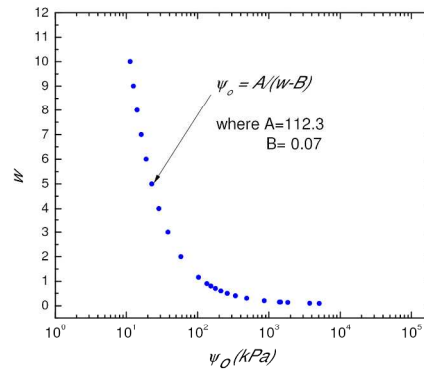48
49
50
51
52
53
54
55
56
57
58
59
60

Fig. 10

Methodology for determining entrance pore diameter, de, from cumulative pore-size distribution

215x279mm (290 x 290 DPI)

1
2
3
4
5
6
7
8
9
10
11
12
13
14
15
16
17
18
19
20
21
22
23
24
25
26
27
28
29
30
31
32
33
34
35
36
37
38
39
40
41
42
43
44
45
46
47
48
49
50
51
52
53
54
55
56
57
58
59
60

$$\psi_o = A/(w-B)$$

where A=112.3
B= 0.07

$\psi_O (kPa)$

W

Fig. 11

Relationship between osmotic suction, ψ_o and water content, w, based on Peroni and Tarantino (2004) model
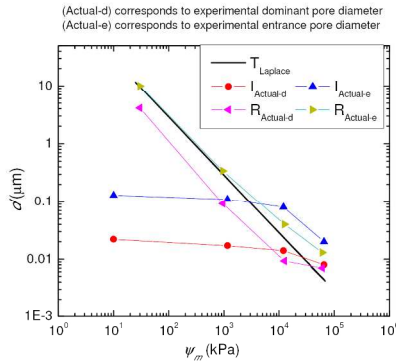
215x279mm (290 x 290 DPI)

1
2
3
4
5
6
7
8
9
10
11
12
13
14
15
16
17
18
19
20
21
22
23
24
25
26
27
28
29
30
31
32
33
34
35
36
37
38
39
40
41
42
43
44
45
46
47
48
49
50
51
52
53
54
55
56
57
58
59
60

Fig. 12

Relationship between matric suction, ψ_m, and pore diameter, d, for the Intact and Reconstituted specimens of the swelling clay SC1

215x279mm (290 x 290 DPI)

1
2
3
4
5
6
7
8
9
10
11
12
13
14
15
16
17
18
19
20
21
22
23
24
25
26
27
28
29
30
31
32
33
34
35
36
37
38
39
40
41
42
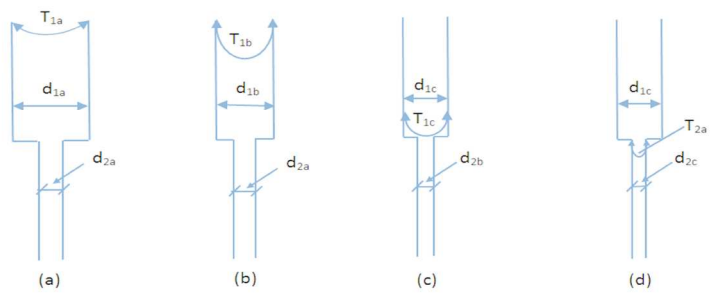43
44
45
46
47
48
49
50
51
52
53
54
55
56
57
58
59
60

Fig. 13

Mechanism of desaturation and shrinkage in Swelling Clays

215x279mm (290 x 290 DPI)

1
2
3
4
5
6
7
8
9
10
11
12
13
14
15
16
17
18
19
20
21
22
23
24
25
26
27
28
29
30
31
32
33
34
35
36
37
38
39
40
41
42
43
44
45
46
47
48
49
50
51
52
53
54
55
56
57
58
59
60

(Actual-d) corresponds to experimental dominant pore diameter
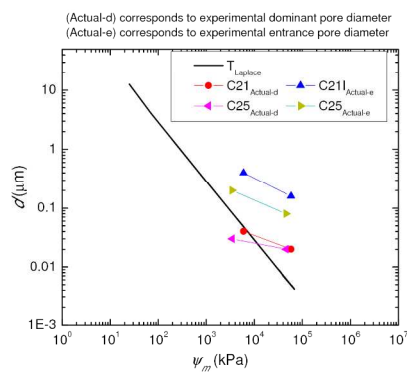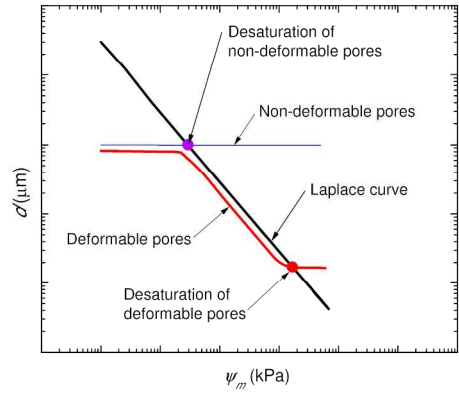(Actual-e) corresponds to experimental entrance pore diameter

Fig. 14

Relationship between matric suction, ψ_m, and pore diameter, d, for Compacted specimens of swelling clay SC1

215x279mm (290 x 290 DPI)

Fig. 15

Deformable capillary tube concept

215x279mm (290 x 290 DPI)